Proceedings of GT2006
ASME Turbo Expo 2006: Power for Land, Sea and Air
May 8-11, 2006, Barcelona, Spain

GT2006-90067

EFFECTS OF SAND INGESTION ON THE BLOCKAGE OF FILM-COOLING HOLES

W. S. Walsh, and K. A. Thole
Mechanical Engineering
Virginia Polytechnic Institute and State University
Blacksburg, VA 24061

Chris Joe
Pratt & Whitney
United Technologies Corporation
East Hartford, CT 06108

ABSTRACT

Gas turbines are often subjected to conditions where dirt and sand are ingested into the engine during takeoffs and landings. Given most aero engines do not have filtration systems, particulates can be present in both the main gas path and coolant streams. Particulates can block coolant passages and film-cooling holes that lead to increased airfoil temperatures caused by reduced coolant available for a given pressure ratio across the cooling holes.

This study investigated the effects of sand blockage on film-cooling holes placed in a leading edge coupon. The coupon was tested to determine the reduction in flow parameter for a range of pressure ratios, coolant temperatures, metal temperatures, number of cooling holes, sand amounts, and sand diameters. Depending upon conditions, blockages characterized by reduced coolant flow can be as high as 10%.

INTRODUCTION

Turbine engines used for propulsion operate in a variety of environments that affect their component performance and life. One specific environment of interest is where ingestion of small particles, particularly sand, takes place. While large particles can cause catastrophic damage, small particles of dust and sand in the air can also affect engine performance. During takeoff, the engine is operating at elevated temperatures and flowrates. The high flowrates into the engine cause an unsteady vortex that forms in front of the nacelle and, if the environment is such, it will entrain sand into the compressor inlet as shown in a numerical simulation by Moroianu et al. [1]. This vortex is visible in Figure 1, where large quantities of sand are being ingested into the engines of a C-17 during takeoff. Typically, gas turbines will receive very short bursts of sand at high concentration levels during takeoffs and landings, and will then operate for long periods with almost no particulates being ingested while the aircraft is at cruise altitude.

The sand-air mixture enters the compressor at moderate concentrations and as the air flows through the compressor and increases in density while the sand does not, the volume ratio of

Figure 1. Sand ingested into a C-17 during takeoff.

sand to air increases, as discussed by Kim et al. [2]. In different locations within the compressor, air is bled through the combustor bypass to provide cooling for turbine parts. Some particles, particularly the small ones, will be diverted through the combustor bypass as observed in engine sand tests conducted by Dunn et al. [3]. During the travel through the compressor and combustor bypass, the sand affects many surfaces and can break up into many small particles, as shown by Schneider et al. [4] and also by Batcho et al. [5]. The combustor bypass air supplies coolant to blades and vanes that are in the turbine. The bypass air is fed to inside passages of vanes and blades for convective cooling, and is then directed through holes in the airfoil surfaces for film-cooling.

To design an engine with reasonable maintenance intervals, high performance, and high efficiency, it is necessary to effectively use the combustor bypass air as coolant for the turbine components. When internal cooling passages and film-cooling holes are blocked in turbine components, the cooling necessary to maintain component temperatures at reasonable temperatures can not be sustained. Considering that the slip velocity between the sand and coolant is relatively small, the particulate temperatures increase rapidly through radiation by the hot surfaces. In some cases, extreme temperatures of the

metal surfaces in an airfoil can cause melting of the sand particles and increase the probability that the particles will adhere to the coolant passages. As sand blocks a coolant passage or coolant hole it reduces the overall supply of coolant flow and creates a localized hot region in the blade. As sand adheres to the surface of a passage it also acts as an insulating material reducing the heat transfer from the metal surface to the coolant thereby further increasing part temperature. The combination of reduced convection, increased thermal resistance, and decreased mass flow cause the metal temperature to further increase resulting in a reduction in service life. This was found by Kim et al. [2] for volcanic ash ingestion. Sand ingestion also causes erosion that can result in lower adiabatic efficiency. A study on sand ingestion in an axial fan by Ghenaiet et al. [6] indicated that after a 6 hour sand ingestion test, there was a 7% reduction in adiabatic efficiency.

This paper provides a methodology and test results conducted on a simple test coupon representative of an airfoil leading edge, which is one of the most difficult areas to cool and one of the most susceptible areas to sand blockage as shown in studies on external deposition tests by Tabakoff et al. [7] and Kim et al. [2]. The test coupon contains an array of film-cooling holes with a typical diameter and orientation as seen in a leading edge of a turbine vane. The coupon was tested for a number of different conditions by varying the number of coolant holes, the sand amount and character, pressure ratio, coolant temperature, and metal temperature.

NOMENCLATURE

%RFP	percent reduction in flow parameter
D	cooling hole diameter
f	friction factor
FP	flow parameter
k	minor loss coefficient
L	cooling hole length
$\dot{m}$	mass flow
P	pressure
PR	pressure ratio
R	gas constant for air
SCMM	standard cubic meters per minute
T	temperature
V	average cooling hole velocity

Greek

Φ	effectiveness
ρ	coolant density

Subscripts

C	cold conditions
CC	cold test – cold baseline
H	hot conditions
HH	hot test – hot baseline
HC	hot test – cold baseline
O	baseline conditions with no sand
OC	total property of the coolant
∞	freestream conditions

PAST RELAVANT STUDIES

There have been numerous studies by Schneider et al. [4, 8, 9, 10] and Ghenaiet et al. [6] that show methods of particle separation in combustor bypass air. To the authors' knowledge, however, propulsive turbines do not generally have filtering systems due to space and weight constraints.

The mechanisms of particle transport and deposition are important to understand so that relevant conditions can be matched in an experimental environment. In an engine, the friction drag from the high-speed coolant primarily keeps sand particles in an aerosol state. The particles move at nearly the same velocity as the air through the coolant system. However, given their mass and subsequently higher momentum, the particles do not necessarily follow the coolant streamlines through the turns nor through the arrays of pin fins, ribs, and film cooling holes. Instead, the particles impact surfaces where there are several forces that will dictate whether or not the particle will adhere to the surface. A restitution force is generated by the slight deflections in the surfaces of the particle and of the wall at impact. The magnitude of the restitution force is dependent on the coefficient of restitution and impact angle. The higher the velocity and the more normal the particle impacts the surface, the higher the rebound force. A thermophoresis force is generated by the difference in molecular motion in areas of high temperature gradients, as discussed by Friedlander [11]. Thermophoresis causes a force to shift the particles away from areas of high molecular motion, (hot regions). The London-van der Waals force is an attractive force generated by atomic dipoles that acts over very short distances. Van der Waals forces are attractive between the wall and the particle. If the restitution force and the thermophoratic force are higher than the van der Waals force, the particle will rebound. If not, the particle will adhere to the surface. In addition to these forces, surface roughness increases the probability of particle adhesion.

The combination of extreme temperature and residence time can lead to sand even melting inside the turbine component. The residence time for a particle increases every time the particle impacts the wall. Schneider et al. [4, 8, 9, 10] have shown that in areas of relatively high turning particles may have residence times much longer than if the particles had followed the flow streamlines. If a particle's residence time is high enough, simple calculations, similar to those shown by Kim et al. [2] indicate a rapid rise in the particle temperatures. As discussed by Friedlander [11], the melting point can significantly decrease as the grain size decreases. This is similar to the lower than expected melting points of volcanic ash found by Kim et al. [2]. The restitution force is dramatically reduced when the particle is melted causing the particle to adhere to the surface.

When particles adhere to a surface, a chain reaction is started that could have severe effects. When a particle adheres to a surface, it increases the metal temperature by reducing the coolant flow, and increases the thermal resistance between the wall and the coolant air, as discussed by Kim et al. [2]. The higher metal temperature in turn leads to higher temperatures of the particles adhered to the wall increasing the likelihood that more particles will adhere. Studies by Kim et al. [2] indicate that increased metal temperatures significantly enhance adhesion rates. Both Wenglarz et al. [12] and Kim et al. [2] have shown that after the metal temperature reaches a certain value, the adhesion characteristics are nonlinear and the rate at which adhesion continues increases rapidly.

With increasing temperatures of gas turbine engines and the development of new cooling designs, it is critical to

evaluate the effects of ingested sand particles. The reduction of flow to the coolant passages and film-cooling holes can quickly cause part temperatures to increase, significantly reducing part life. Engines are most susceptible to sand ingestion during critical times such as takeoffs and landings. Given this information, it is necessary to identify and quantify the parameters that most affect sand deposition.

BACKGROUND

There are many different ways to characterize sand blockage in a film-cooling hole. The gas turbine industry generally uses a term called flow parameter (FP) for overall estimates of coolant flow supplied to a particular airfoil. The flow parameter, shown in equation 1, is a non-dimensional term that is the ratio of momentum force to pressure force, as discussed by Hill et al. [13].

$$FP = \frac{\dot{m}\sqrt{T_{OC}R}}{P_{OC}D^2} \quad (1)$$

When the flow parameter and temperatures are matched to realistic engine conditions, the residence time of the air in a component will match the residence time in the airfoil component during operating conditions. This is true even if the overall pressure ratio is not matched, as discussed by Kim et al. [2]. For a particular airfoil operating at a given coolant temperature, there is a distinctive relationship between the flow parameter and pressure ratio. This flow parameter will only vary if the coolant temperature (specific heat) significantly changes or if the geometry is significantly changed, as in the case with sand blockage in a film-cooling hole. The results presented in this paper are given in terms of a reduction of the flow parameter in the case with sand relative to that which occurs for clean cooling holes.

TEST COUPON AND METHODOLOGY

The test coupon used for these studies was designed to replicate characteristics of the leading edge of a turbine airfoil. Two coupons were manufactured with identical geometries except for the number of holes to allow direct comparisons. The holes were manufactured for the coupon using laser drilling. The 60-hole coupon was designed for a given range of pressure ratios and to allow for matching metal and coolant temperatures to those found in actual engines. The coolant holes had a 90° compound angle opposing the direction of the internal flow inlet as shown in Figure 2. The coupons were made from Inconel 625, which has similar characteristics as airfoil metals..

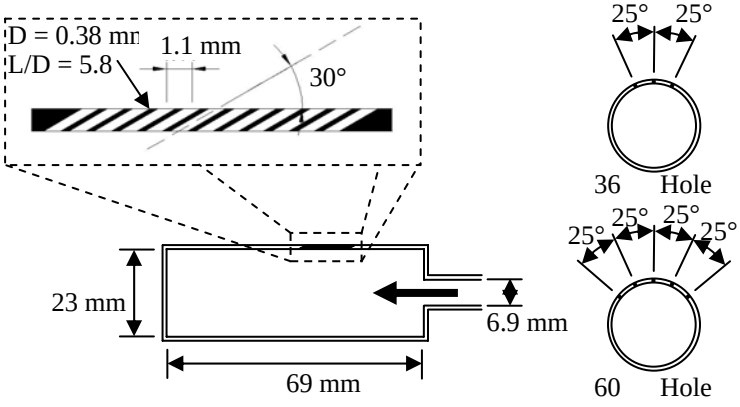

Figure 2. The 60-hole and 36-hole test coupons were designed to simulate the leading edge showerhead.

The test rig consisted of a compressed air coolant supply, sand delivery system, a kiln, and a double-pass heat exchanger, as shown in Figure 3. The instrumentation used is shown in Figure 4. The coolant was supplied to the coupon by a compressed air supply that was provided by the Virginia Tech Physical Plant. A precision pressure-regulating valve was used to insure a controlled, constant coolant pressure. Downstream of the pressure regulator, the coolant entered a laminar flow element to measure the coolant mass flow supplied to the coupon. The laminar flow element had an accuracy of ±0.86% of the actual reading. The flow then passed through an eductor used for sand delivery and then into the coupon.

The sand delivery system consisted of an eductor, a valve, and the piping necessary to deliver the sand-air mixture to the coupon. The eductor, used to mix the sand into the coolant, contained a nozzle designed to entrain the sand and a feed port above the nozzle to gravity feed the sand. A ball valve was placed on top of the sand feed located far enough outside the kiln so that sand could be safely added while the kiln was heating the coupon. The eductor was located as close as possible to the coupon to minimize deposits on the supply tube walls. The location chosen was approximately 40 cm upstream of the coupon, as shown in Figure 3.

The ability for the eductor to drive the sand into the coupon was dependent on the pressure ratio across the eductor. The mass flows required for the target pressure ratio ranges in the coupon were somewhat higher than those indicated for this eductor design. Therefore, a bypass line with a control valve was used to set the pressure ratio across the eductor above a minimum threshold pressure required to move the sand. The bypass line allowed the mass flow to set the pressure ratio.

Since coolant and metal temperatures are important parameters, temperatures were matched to realistic engine operating conditions. To match the coupon metal (980-1040°C) and coolant temperatures (650-700°C) to those found in turbine engines, a ceramic kiln that supplied a maximum of 6.9 kW was used. The kiln had several ports so that different parts of the test rig could protrude through the firebrick liner. A programmable electronic controller was used to ramp up and to maintain the kiln temperature within ± 5°C.

Since the coolant air traveled through a tube before it reached the coupon, its temperature depended on the kiln temperature and the heat transfer coefficient inside the supply tube for that particular flow rate. Depending upon the flow rate through the coupon, the temperature of the coolant could vary significantly without some form of control. To maintain the desired coolant temperatures, a double-pass heat exchanger was

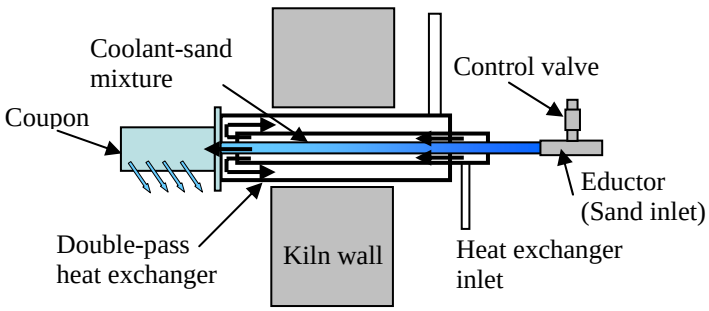

Figure 3. The test rig for the sand ingestion tests included a sand delivery system.

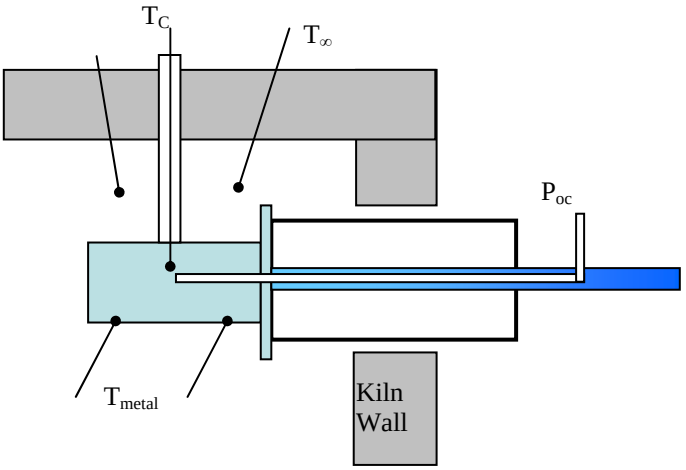

Figure 4. The effectiveness was determined so that the metal temperature could be determined at engine temperatures.

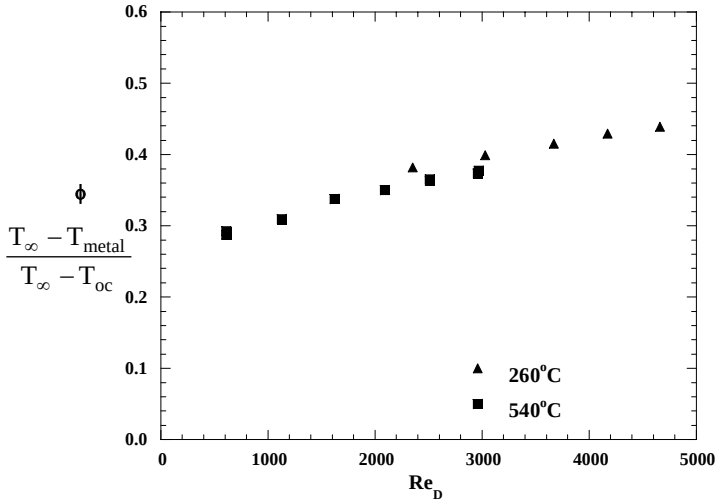

Figure 5. Effectiveness of the 60 hole coupon as a function of Re for various temperatures.

constructed around the coolant supply tube, as shown in Figure 3. The heat exchanger was designed so that compressed air could be supplied to it and vented to atmosphere, outside of the kiln to reduce the load on the kiln. With the extra control of the heat exchanger, all of the coolant temperatures and metal temperatures were matched to that of turbine conditions.

A combination of pressure transducers and thermocouples were used to measure several key parameters throughout the test rig including the coolant temperature, pressure ratio, coolant mass flow, and metal temperature of the coupon. The thermocouple and pressure probes used to measure the temperature and pressure inside the coupon were fed through tubes such as the port, illustrated in Figure 4, between atmospheric air and high-pressure air could be located outside the kiln. The coolant temperature was monitored with a Type K nickel-chrome sheathed thermocouple probe. The relatively large area ratio of the plenum to the coolant holes (63:1 for the 60-hole coupon) and the relatively low velocity, allowed the pressure measurements inside the coupon to be treated as the total coolant supply pressure.

It was not possible to directly measure the metal temperatures because of the mounting difficulties of a thermocouple onto the coupon. As such, the metal temperature was calculated through an effectiveness parameter. Effectiveness is defined in equation 2 and is a dimensionless ratio that relates the known temperatures of the kiln air (T_∞) and coolant air (T_{oc}) with the temperature of the metal for various Reynolds numbers.

$$\phi = \frac{T_\infty - T_{metal}}{T_\infty - T_{oc}} \qquad (2)$$

Effectiveness tests were conducted at temperatures in which it was possible to mount thermocouples to the coupon. These effectiveness values were then used for the higher temperature tests to deduce the metal temperatures. Effectiveness tests were conducted for a range of Reynolds numbers. Thermocouples were mounted in two locations along the middle row of cooling holes, spaced 6 mm away from the nearest cooling hole, as shown in Figure 4. The kiln air temperature was also monitored with a type K thermocouple located directly above the coupon (away from the cooling). The coolant air was measured with the coolant thermocouple inside the coupon. The coupons were tested at two different kiln temperatures (260°C and 540°C) and several different Reynolds numbers. The results confirmed that the effectiveness was a function of Reynolds number and independent of temperature, as shown in Figure 5. The effectiveness levels are lower than expected for a typical turbine airfoil because there were no internal cooling features. The dependence on Reynolds number in conjunction with the independence on temperature allowed the effectiveness to be used at all kiln temperatures to deduce the coupon temperature.

As was previously stated, the flow parameter calculated using equation 1 was used to gage the cooing hole blockage. A baseline flow parameter (FP) versus pressure ratio (PR) curve was measured, as shown in Figure 6, for the 36 and 60-hole coupons. Note that the pressure ratio is the ratio of the internal coolant supply pressure to the external static pressure. The difference between the flow parameters from the 36 and 60-hole coupons is from uncertainty including manufacturing tolerances. The manufacturing tolerance on the hole diameter was ± 6.35×10^{-5} m. Because flow parameter is a function of temperature, another baseline curve was measured at engine temperatures.

The flow parameter for a film-cooling hole can be approximated by assuming one-dimensional flow. The pressure ratio of the coupon total pressure to the atmospheric pressure can be calculated as shown in Equation 3.

$$PR = 1 + \left(f \frac{L}{D} + k_{inlet} + k_{exit} \right) \frac{\rho V^2}{2 P_\infty} \qquad (3)$$

The first term is the viscous loss in a smooth pipe using the Blasius correlation for friction factor. The second term is the total pressure loss due to a square-edged entrance condition into the film cooling, using a value for k_{inlet} of 0.4. The third term is the total pressure loss due to a square-edged exit loss, using a value for k_{exit} of 0.6. From this equation, the velocity is calculated and used to determine a flow parameter. For a pressure ratio of 1.4, the Reynolds number was 6875, the friction factor was 0.0347, and the calculated exit velocity was 202 m/s. The prediction works well as shown by the comparison with actual data from the 36 and 60-hole coupon.

Different flow parameters occur for heated and cold conditions. These differences are due to changes in viscosity as well as slight cooling hole expansion that occurs due to heating (expected to be a 2% increase in flow area). In this study, we

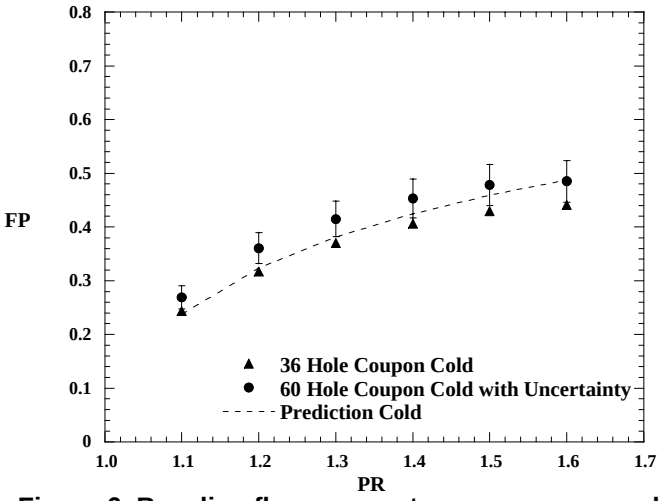

Figure 6. Baseline flow parameters were measured for both coupons and compared to a prediction.

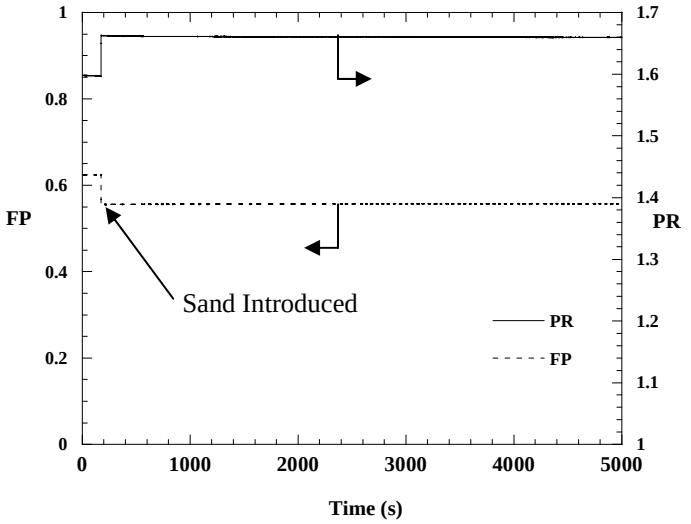

Figure 7. The flow parameter and pressure ratio stabilize a few seconds after sand is introduced and remain steady.

are primarily interested in the percent reduction in flow parameter (%RFP). The percent reduction in flow parameter can be defined several different ways, as we have done in this paper, depending upon which baseline is used. In all cases, however, the %RFP is based on the final resulting pressure ratio (after sand was injected). One definition is to compare the percent reduction in flow parameter under cold conditions whereby the cold baseline is used as a reference and only a cold (room temperature) test is conducted. Determining the percent reduction in flow parameter $\%RFP_{CC}$ (cold sand test – cold baseline), shown in Equation 4, can then be used to estimate the reduction of part flow for a given sand flow. Under cold conditions, FP_0 is the baseline flow parameter and FP is the flow parameter after sand has clogged the holes.

$$\%RFP = \frac{FP_0 - FP}{FP_0} \tag{4}$$

For heated conditions, two definitions could be used. The first method, which will be called $\%RFP_{HH}$ (heated sand test – heated baseline), uses FP_0 as the baseline flow parameter at heated conditions, and FP as the value at heated conditions just after the sand is released. The second method, which will be called $\%RFP_{HC}$ (heated test – cold baseline), uses the cold baseline value of FP_0 just prior to the test and uses FP as the resulting value after sand has been injected and the coupon has returned to room temperature.

The method of introduction to the test coupon was important because the coupon could have different blocking characteristics based on the release method. For simplicity and repeatability, a slug flow was used to test the blockage characteristics of the coupons. The slug flow was generated by placing a measured sand amount inside an airtight section of pipe connected by a valve to the eductor. When the valve was opened, the sand fell into the eductor and the high velocity jet entrained the sand into the air as a slug flow. After the sand is introduced, there is a step decrease in flow rate and step increase in pressure ratio, as shown in Figure 7. After the sand blocks the hole, the flow parameter and pressure ratio remain at a steady state value. This ending value of pressure ratio and flow parameter were used deduce the flow reduction (%RFP).

The sand amounts used in the coupon tests were deduced by determining sand amount needed to match flow blockage levels to that occurring in actual engine components. In an actual engine, the sand concentration would be a function of density ratio (pressure ratio) as discussed by Kim et al. [2].

As a part of the testing methodology, the moisture content of the sand was minimized. The first reason is that the humidity in the laboratory could not be controlled, and therefore daily variations would have affected the sand adhesion characteristics. This was shown to occur through testing. The second reason is that desert regions where sand ingestion is common have low humidity levels. The sand was kept in an oven maintained at 200°C for at least 4 hours prior to testing.

Prior to all tests, the coupon was cleaned until the original baseline flow parameter / pressure ratio relationship was verified. The coupon was cleaned using a combination of compressed air and small drill bits pushed through the cooling holes. For cold sand ingestion tests, the baseline flow parameter was measured at the target pressure ratio, and then the dried sand was injected into the system through the use of the eductor. After a few seconds the system stabilized and remained blocked indefinitely, as was previously indicated by Figure 7. For the heated tests, as was stated, a kiln was used to raise the temperature of the metal and coolant within a realistic range to satisfy the residence time criteria as described by Kim et al. [2]. The target temperature ranges were 1010 ± 30°C for the metal temperature, and 680 ± 30°C for the coolant temperature. For the heated testing procedures, initially the room temperature baseline flow parameter / pressure ratio was verified. The kiln was then turned on and allowed to ramp up to the target temperature with the coupon being actively cooled. After the coolant and metal temperatures were steady and within the desired ranges, dried sand was added to the sand feed port above the eductor and injected into the system. The $\%RFP_{HH}$ was calculated by taking the flow parameter just after sand injection and comparing it to the heated baseline flow parameter at the same ending pressure ratio. The coupon was then cooled down to room temperature and another measurement was made and compared to the cold baseline in order to get a $\%RFP_{HC}$.

Uncertainty Analysis

An uncertainty analysis was performed on several key parameters using the partial derivative method, shown in Table 1. The uncertainty of the pressure ratio was calculated to be 1.1 ± 6.6 x 10^{-5} and 1.6 ± 9.6 x 10^{-5}. The uncertainty of the flow parameter was calculated to be between 4.6% and 8.0% dominated by the bias uncertainty of the pressure transducer of the laminar flow element. The uncertainty of the %RFP was a maximum under the heated conditions at a low pressure ratio where the measurement was 8.5 ± 0.85%. Under heated conditions, the accuracy of the metal temperature through the effectiveness method was calculated to be 1010 ± 32°C. The uncertainty in the sand measured for each test was estimated to be 0.5 ± 0.001g. A repeatability study was conducted to determine how many identical cases were required to achieve a reasonable confidence interval on the experimental average %RFP. A series of 25 cases with matching pressure ratios and sand amounts were conducted at room temperature. A 95% confidence interval was calculated from the standard deviation of the averages from each sample size of five samples. It was found that the ideal balance between a small confidence interval and a large number of tests was to conduct three tests at each pressure ratio and sand combination. This resulted in a confidence interval of 6.9%.

Table 1. Uncertainties for Parameters

	60-Hole Coupon (cold)		60-Hole Coupon (heated)	
PR	1.1	1.6	1.1	1.6
PR	0.55%	0.37%	0.55%	0.33%
Mass flow	5.2%	6.4%	6.3%	3.2%
FP	6.2%	7.4%	7.2%	4.6%
%RFP	0.23%	0.05%	0.85%	0.35%
ϕ	-	-	1.2%	1.5%
Sand	0.20%			

SAND CHARACTERIZATION

The sand types tested were standard test sands chosen to have similar properties as the sand found in desert and arid regions. While naturally occurring sand may have variations in its properties, the test sands were used for consistency. The parameters that were considered important were size distribution, chemical composition, and sand grain density.

Sand diameter is important because in conjunction with sand grain density, it dictates how well the sand will follow streamlines in curved or obstructed passages. Three different sand diameter distributions were tested. The size distribution was measured with a laser diffraction particle size analyzer. The size distributions measured for the two test sands, shown in Figure 8, compare well to the specifications provided by Powder Technology, Inc. The ISO fine test dust was found to have the lowest average diameter followed by the ISO Coarse test dust and then the VT test dust. The VT test dust was created by using a sieve shaker and a series of sieves. The sieves were set up to filter out many of the particles less than 75 µm from the ISO Coarse test dust.

Sample	Density (g/cm^3)	Mean Diameter (µm)
Test Dust ISO 12103-1, A2 Fine	2.71	18.5
Test Dust ISO 12103-1, A4 Coarse	2.68	37.3
VT Sieved Test Dust	2.68	50

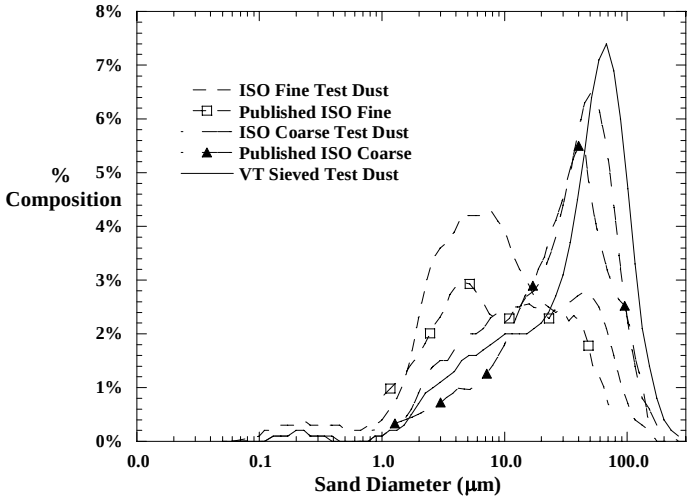

Figure 8. The particle size distributions were found to have a major impact on the %RFP for all cases.

Sand grain densities were measured with a pycnometer, with a maximum standard deviation of 0.0051 g. The densities for all three sands, shown in Figure 8, were very similar. The sand chemical composition was quantified because at the high temperatures that gas turbines operate, it is possible to melt the sand. The composition was qualitatively analyzed with an SEM EDAX system. The EDAX system reports a bulk power spectrum over the entire sample as well as results for particular grains. While the grains vary over a range of different compounds, the bulk power spectrum, shown in Figure 9, indicate that the test dusts are crushed granite. The analysis of each of the samples agree with the manufacturer's specification stating that it contains different phases of quartz (SiO_2) up to approximately 68-76%. The other major constituent is aluminum oxide (Al_2O_3) between 10-15%, with traces of iron oxide (Fe_2O_3), sodium silicate (Na_2O), lime (CaO), magnesium oxide (MgO), titanium dioxide (TiO_2), and potassium oxide (K_2O), in descending concentration.

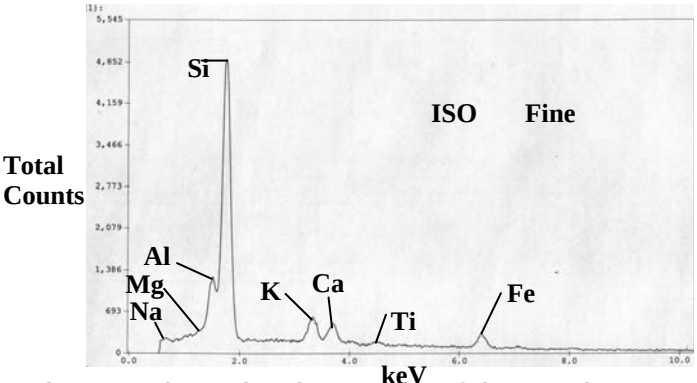

Figure 9. The molecular content of the test dusts indicates that the samples are crushed granite.

It is known that particle size and chemistry affects the melting point of sand made up of a mixture of materials as discussed by Dunn et al. [3]. The crushed granite has many different constituents that, given their size, have a lower melting point than larger samples of the same material. To establish an estimate of the melting temperatures, sand samples were exposed to temperatures ranging from 930°C to 1090°C for 30 minutes, and then removed. Figure 10 shows the samples after their tests at a given temperature. The sample at 930°C has a slight coloration change from what is seen at room temperature, indicating that melting had begun; however, no other major changes. The sample at 980°C has begun to form soft bonds with the material in close proximity. While the sample at 980°C formed larger agglomerate than the sand at 1040°C, the sample at 980°C was easily broken apart, and looked much like the sample at 930°C when this is done. The sample at 1040°C had a significant color change and solid particles much larger than the original sand. These darker particles also could not be broken apart, unlike the samples at lower temperatures. The sample at 1090°C melted and formed a single piece that was solid and could not be broken.

After determining what temperature the sand begins to agglomerate, it is important to determine how quickly the particle can reach the surface temperature while flowing through the coupon. A simplified analysis was performed where it was assumed that all of the energy transferred to the particle was from radiation. Convection was ignored because the temperatures were high enough and the slip velocity was low enough that convection was negligible. In addition, particle impacts were ignored, although this may have served to heat the particle faster. The residence time in the coupon was estimated to be 0.01 s assuming a straight path out of the coupon. This is considered a low estimate since it has been shown by Schneider et al. [4, 8, 9, 10], that particles can have a much longer residence time than the air that carries them depending on the path taken. From these approximations it was found that after 0.01s the sand temperature is 820°C from a starting temperature of 675°C for a coupon metal temperature of 1010°C.

DISCUSSION OF RESULTS

Results from this paper include sensitivity studies on metal temperature, coolant temperature, mean sand diameter, and pressure ratio. Tests were conducted at room temperature at different pressure ratios to determine the effects of sand amounts, sand diameter, and number of cooling holes on the $\%RFP_{CC}$. Heated tests were conducted to determine the combined effect of coolant and metal temperature on the $\%RFP_{HH}$ and $\%RFP_{HC}$. Lastly, the metal temperature and coolant temperature were varied independently to determine its effect on the $\%RFP_{HH}$ and $\%RFP_{HC}$ at a given pressure ratio and sand amount.

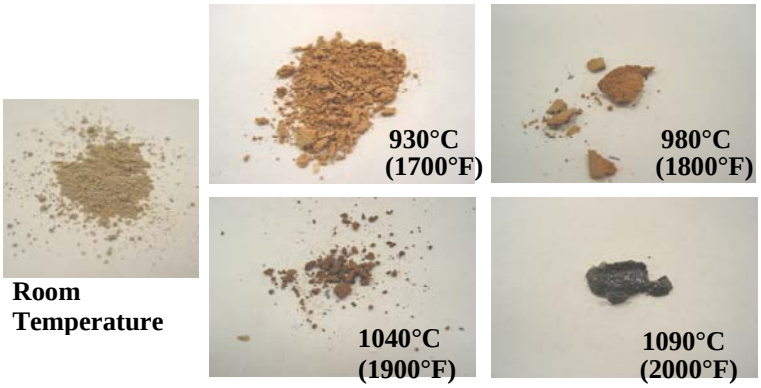

Figure 10. Dusts similar in composition to those found in arid regions melt at moderate temperatures.

Room Temperature Results

This section will present the results obtained with the 36 and 60-hole coupon at room temperature with varying pressure ratios, sand amounts, sand diameters, and number of cooling holes. For the 36-hole coupon, varying amounts of ISO Fine test dust were injected at different pressure ratios at room temperature. Figure 11 shows the distribution of the raw test data for a sand amount of 0.3 grams. Figure 11 indicates that for a given pressure ratio, more sand resulted in a larger $\%RFP_{CC}$. For a constant sand amount the $\%RFP_{CC}$ is lower at higher pressure ratios. The reason for these lower blockages at higher pressure ratios was that there was more coolant mass flow for a high pressure ratio as compared with a low pressure ratio. The higher coolant mass flow reduced the residence time in the coupon. The higher sand velocities also caused more particles to rebound off surfaces most likely causing the sand to break into smaller diameter particles. Smaller particles would have less likelihood of adhering to the surface of the cooling holes. The increased likelihood of rebounding and the lower residence time reduced the probability of a given grain adhering to the wall. Figure 11 indicates that there is a larger relative decrease in $\%RFP_{CC}$ between a pressure ratio of 1.1 and 1.2 than there is between 1.2 and 1.5. There is another sharp decrease in $\%RFP_{CC}$ between a pressure ratio of 1.5 and 1.6.

As seen in Figure 11, there is a consistency in the flow blockage characteristics between tests for different sand amounts. Figure 12 shows the same curves of $\%RFP_{CC}$ normalized by the sand amount. Figure 12 shows that for a given pressure ratio, the normalized $\%RFP_{CC}$ is nearly the same. This finding indicates that at room temperature, for a consistent sand type and pressure ratio, $\%RFP_{CC}$ is nearly a

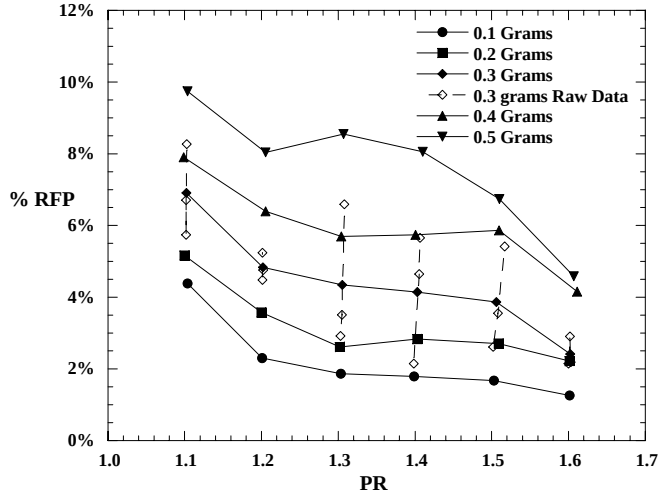

Figure 11. Increasing sand amount increases %RFP for a given pressure ratio (ISO Fine, 36-hole coupon).

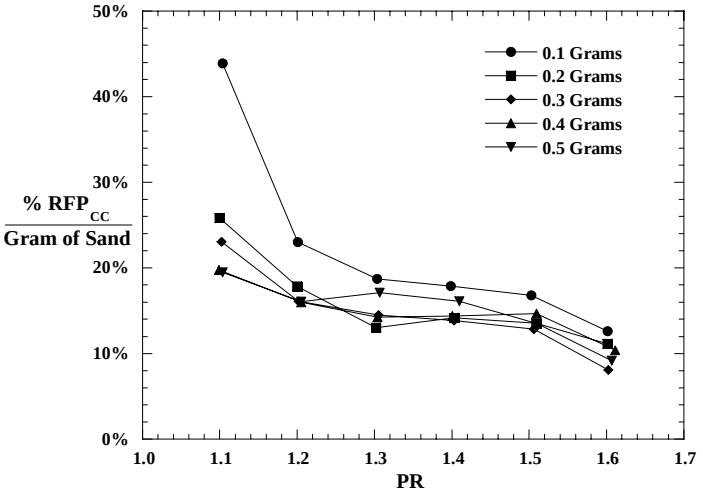

Figure 12. The %RFP has a nearly linear dependence on the sand amount (ISO Fine, 36-hole coupon).

linear function of sand amount. There is one curve in Figure 12 that has a slight disagreement with this trend. The lowest sand amount of 0.1 grams has a larger blocking per gram of sand.

By testing a coupon similar to the 36-hole coupon, but with a total of 60 cooling holes, assessments could be made as to whether the total coolant flow area had an effect. Over a range of pressure ratios, 0.5 grams of ISO Fine test dust was injected into the 60-hole coupon. The 60-hole coupon had 67% more coolant flow area than the 36-hole coupon. Figure 13 shows the effect of increased flow area on the $\%RFP_{CC}$ over a range of pressure ratios. In addition to the two curves with the data points, a prediction of the blockage was made using the results from the 36-hole coupon by considering a simple cooling flow ratio between the two coupons. Lower blockage levels were observed in the 60-hole coupon and were not predicted using the results from the 36-hole coupon. The reason for this discrepancy was primarily because of the increased mass flow through the inlet tube for the 60 hole coupon. The supply tube for both the 36 and 60-hole coupons had the same diameter resulting in a supply velocity exiting the tube for the 60-hole coupon to be much higher than for the 36 hole coupon. This higher supply velocity caused the particles to impact the opposite end of the coupon (capped off portion) and fall out rather than exiting the cooling holes.

For the 60-hole coupon, the effect of sand diameter was also evaluated. This parameter is important because as the size distributions showed, individual sand grains can be on the order of one percent the size of the hole to nearly half the hole diameter. The three sands that were tested were the ISO Fine, ISO Coarse, and the VT sand that had mean diameters of 18.5, 37.3, and 50.0 μm respectively. Tests indicated that at room temperature the $\%RFP_{CC}$ was directly dependent on average sand diameter, and increased with increasing diameter as shown in Figure 14. The increased blockage with increasing sand diameter is because of the increase in the number of larger particles. These larger particles had a lower velocity than the smaller particles and therefore were less likely to rebound off surfaces after impact. In addition, when the larger particles adhered to a surface they had more of an effect because they blocked more flow area than the smaller particles.

Figure 15 shows the same data as in Figure 14, but with lines of constant pressure ratio and as a function of sand diameter. In Figure 15 there is also one series of data that

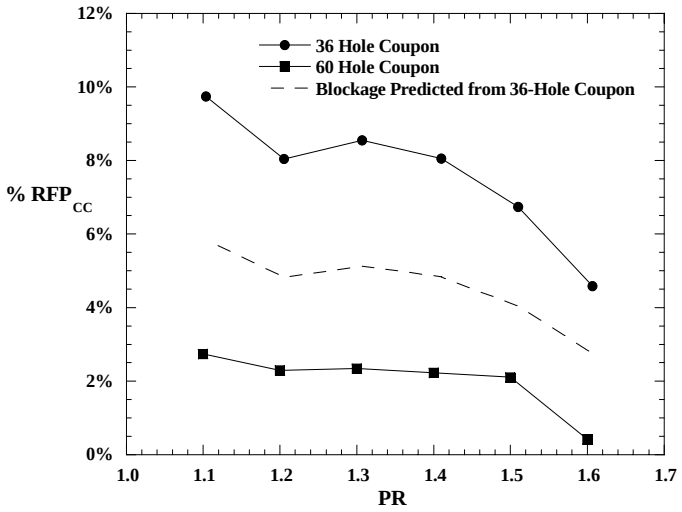

Figure 13. The number of coolant holes has a non-linear effect on the %RFP (0.5 g, ISO Fine test dust).

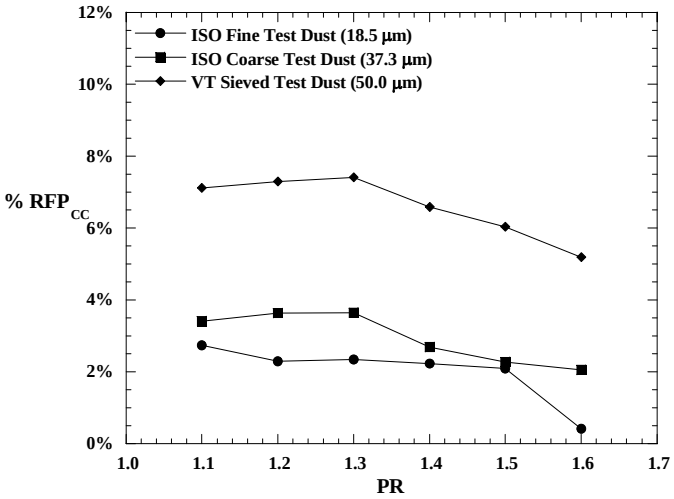

Figure 14. Increasing the average particle size results in increasing blockage (0.5 g, 60 hole coupon).

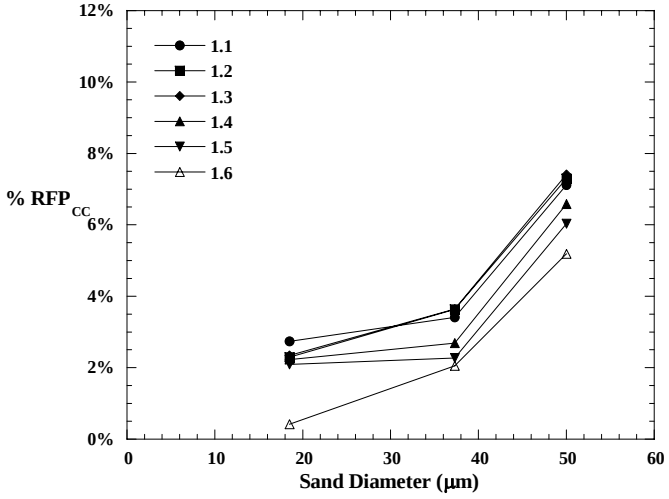

Figure 15. The increase of %RFP is not linear with increasing average sand diameter (0.5 g, 60 hole coupon).

stands out. At the high pressure ratio of 1.6, there is a lower $\%RFP_{CC}$ for all sand types than the other pressure ratios. This is most likely because of the larger mass flow through the cooling holes at a pressure ratio of 1.6.

Heated Experimental Results

Heated tests were conducted using 0.5 grams of ISO Fine test dust to determine the effect of engine-representative temperatures on the sand blocking, as well as determining the sensitivity to varying metal and coolant temperatures. The target metal temperature was between 980°C and 1040 °C, and the target coolant temperature was between 650°C and 700°C. While this range of temperatures was obtainable with the use of the heat exchanger, there were some temperature variations between pressure ratios, as shown in Figure 16.

The comparison between the $\%RFP_{HC}$, $\%RFP_{HH}$, and $\%RFP_{CC}$ for the same 0.5 grams of ISO Fine test dust over a range of pressure ratios is shown in Figure 17. The elevated metal and coolant temperature caused significantly more blockage than occurred at room temperature for the entire range of pressure ratios. Also important to note is that the $\%RFP_{HC}$ was always more than the $\%RFP_{HH}$. This difference between $\%RFP_{HH}$ and $\%RFP_{HC}$ tended to be larger at higher pressure ratios and indicated that the blockage increased as the part cooled to room temperature. The reason the difference between $\%RFP_{HC}$ and $\%RFP_{HH}$ increased at higher pressure ratios was that the local metal temperature increased immediately after the sand blockage. The higher pressure ratio tests required a higher kiln temperature such that after sand blockage occurred, the metal temperatures increased dramatically. This higher metal temperature melted the sand, and increased the blockage. This is consistent with other tests conducted at intermediate coolant and metal temperatures not reported here.

To determine and separate the effects of the coolant temperature and the metal temperature, a series of tests were conducted with a constant metal temperature and a series of tests were conducted with constant coolant temperature. The results from the constant metal temperature of 1010°C and varying coolant temperature are shown in Figure 18. Increasing the coolant temperature caused only a minimal increase in $\%RFP_{HH}$. However, there is a large increase in $\%RFP_{HC}$ from a spike in metal temperature after sand blockage occurred. As

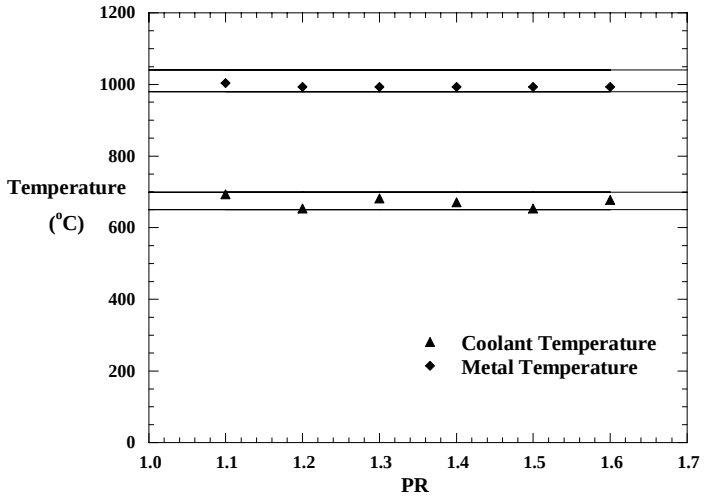

Figure 16. The temperature ranges were met for all pressure ratios, however, there were minor variations between tests (60 hole coupon).

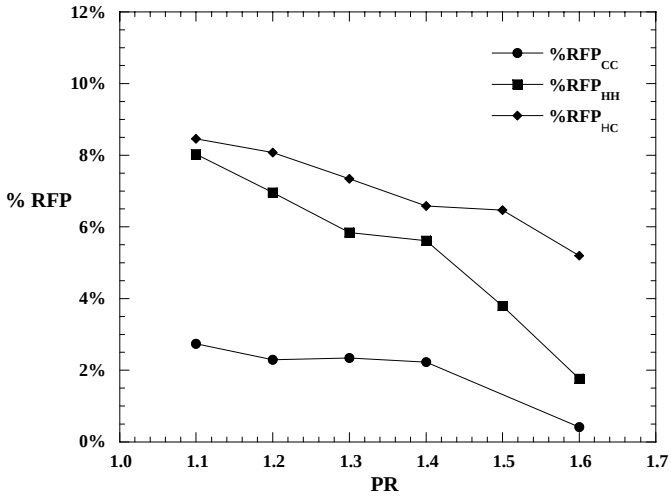

Figure 17. Operating at engine metal temperatures results in higher %RFP (0.5 grams ISO fine 60 hole coupon).

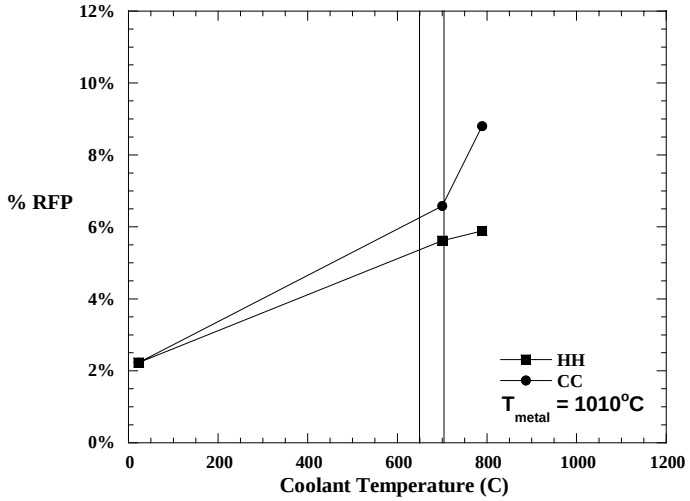

Figure 18. Operating at higher coolant temperatures increases %RFP (0.5 grams, ISO Fine 60-hole coupon, Tmetal = 1010°C).

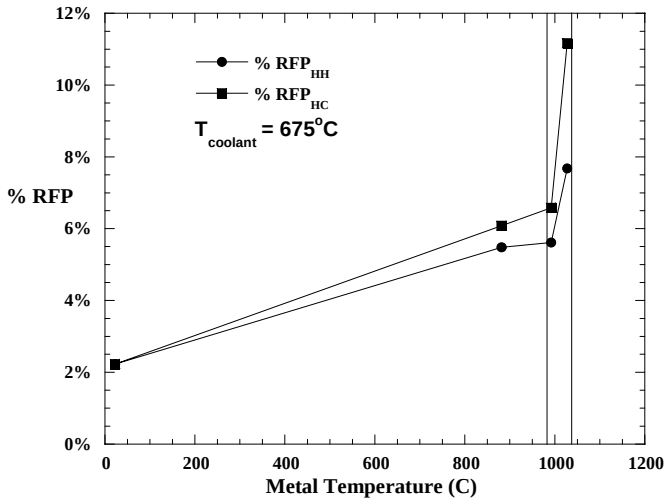

Figure 19. Metal temperature over 1000 °C can cause significant enhancement of %RFP (0.5 g ISO Fine, 60-hole coupon, Tcoolant = 675°C).

discussed previously, the sand injection caused the metal temperature to increase rapidly toward the kiln temperature and began to melt the sand already adhered to the cooling holes. This effect, however is a metal temperature effect, not a coolant temperature effect.

The sensitivity of blockage to metal temperature was determined by maintaining a constant coolant temperature of 675°C and varying the metal temperature. This resulted in a more severe increase in %RFP than the constant coolant temperature tests. Figure 19 shows that the effect of metal temperature on the %RFP indicates a spike between 1000°C and 1080°C. This is due to the melting of the sand as it contacted the metal in the coolant hole. This contact caused immediate melting of the sand and adhesion to the surface.

CONCLUSIONS

Gas turbine engines are designed to operate at high inlet temperatures, but harsh operating conditions need to also be considered. Without sufficient cooling, turbine parts will degrade and cause performance and component loss. Dust and sand from runways is typically ingested into engines during takeoffs and landings. This ingested sand can block coolant passages in airfoils and contribute to degradation of the turbine components. This study determined how a simple array of film-cooling holes reacted to several parameters considered important in sand blocking. Important parameters were determined to be pressure ratio, sand amount, sand distribution, number of holes, and metal temperatures.

The pressure ratio affects the sand blocking by controlling the velocity of the coolant-sand mixture through the cooling holes. A high pressure ratio has higher coolant velocities in the film-cooling holes. This increased coolant velocity increases the particle velocity through the coolant hole making it less likely to adhere to the coolant walls and reducing the chance for hole blockage. For example with the fine test dust, a flow reduction of 10% occurred at a pressure ratio of 1.1 and a reduction of 4.6% occurred for a pressure ratio of 1.6.

The sand amount was determined to affect the blocking by changing the amount of sand per hole that flowed through the coupon. With increasing sand amounts introduced as a slug flow, more sand per hole was injected into the coupon causing more blockage. The sand size distribution was also important in determining the percent reduction in flow parameter. Larger sand diameters gave higher reductions in the flow parameter.

The metal temperature of the coupon was found to be the most significant parameter in this study. As the metal temperature increased beyond 1000°C, the particles most likely melted on impact or melted shortly after impact. The combination of increased metal temperature from the sand already adhered to the surface, and the increased tackiness of the surface caused subsequent particles to have a high probability of adhesion. At a pressure ratio of 1.4, the percent reduction in flow parameter was 5.5%, at 882°C compared with 7.7% for temperatures of 1028°C.

The results presented in this paper represent a beginning to bettering our understanding on the effects of sand blockage of cooling holes in turbine components. These results clearly illustrated the importance of a number of parameters. As new cooling hole designs are derived, it is quite important to consider the environments in which the engine will operate.

ACKNOWLEDGMENTS

The authors gratefully acknowledge the sponsors of the this work, namely United Technologies Corporation - Pratt & Whitney.

REFERENCES

[1] Moroianu, D., Karlsson, A., 2004, “LES of the Flow and Particle Ingestion into an Air Intake of a Jet Engine Running on the Ground,” GT2004-53762

[2] Kim, J., Dunn, M.G., Baran, A.K., Wade, D.P., Tremba, E.L., 1993, “Deposition of Volcanic Materials in the Hot Sections of Two Gas Turbine Engines,” J of Turbomachinery, vol. 115, pp. 641-651.

[3] Dunn, M.G., Padova, C. and Adams, R.M., 1987a, “Operation of Gas Turbine Engines in Dust-Laden Environments,” AGARD-Advanced Technology Aero Engine Components, Paris, France.

[4] Schneider, O., H.J., Benra, F.-K., Dohmen, H. J., and Jarzombek, K., 2005, “A Contribution to the Abrasive Effect of Particles in a Gas Turbine Pre-Swirl Cooling Air System,” GT2005-68188

[5] Batcho, P.F., Moller, J.C., Padova, C., and Dunn, M.G., 1987, “Interpretation of Gas Turbine Response Due to Dust Ingestion,” 1987-GT-112

[6] Ghenaiet, A., Elder, R.L., and Tan, S.C., 2001, “Particles Trajectories Through an Axial Fan and Performance Degradation due to Sand Ingestion,” 2001-GT-0497

[7] Tabakoff, W., and Metwally, M., 1992, “Coating Effect on Particle Trajectories and Turbine Blade Erosion,” *J of Turbomachinery*, vol. 114, pp. 250-257.

[8] Schneider, O., Dohmen, H.J., Reichert, A.W., 2002, “Experimental Analysis of Dust Separation in the Internal Cooling Air System of Gas Turbines”, GT-2002-30240

[9] Schneider, O., Dohmen, H.J., Benra, F.-K., and Brillert, D., 2004, “Dust Separation in a Gas Turbine Pre-Swirl Cooling Air System, a Parameter Variation,” GT2004-53048

[10] Schneider, O., Dohmen, H. J., H.J., Benra, F.-K., and Brillert, D., 2003, “Investigations of Dust Separation in the Internal Cooling Air System of Gas Turbines,” GT2003-38293

[11] Friedlander, S.K., 2000, Smoke, Dust, and Haze Fundamentals of Aerosol Dynamics, (Oxford University Press: NY)

[12] Wenglarz, R.A., and Fox, Jr., R.G., 1990, “Physical Aspects of Deposition from Coal-Water Fuels Under Gas Turbine Conditions,” *J of Turbomachinery*, vol. 112, pp. 9-14.

[13] Hill, P., Peterson, C., 1992, Mechanics and Thermodynamics of Propulsion, (Addison-Wesley Publishing Company: Reading, Massachusetts)

